Orthopaedics & Traumatology: Surgery & Research (2013) 99, 52—59

View metadata, citation and similar papers at core.ac.uk

brought to you by CORE

provided by Elsevier - Publisher Connector

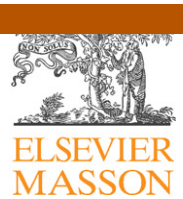

Available online at
SciVerse ScienceDirect
www.sciencedirect.com

Elsevier Masson France
EM|consulte
www.em-consulte.com/en

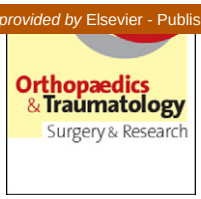

ORIGINAL ARTICLE

Trabecular microarchitecture in established osteoporosis: Relationship between vertebrae, distal radius and calcaneus by X-ray imaging texture analysis

F. Mallard[a,c], B. Bouvard[a], P. Mercier[b], P. Bizot[c], P. Cronier[b,c], D. Chappard[a,*]

[a] *LUNAM, Angers University, Bone remodeling and biomaterials study group (GEROM)—LHEA, IRIS-IBS Biology Institute of Health, Angers Universitary Hospital Center, 49933 Angers Cedex, France*
[b] *LUNAM, Angers University, Anatomy Research Laboratory, Faculy of Medicine, 49000 Angers, France*
[c] *Department of Orthopaedic Surgery,Angers Teaching Hospital Center, 49933 Angers Cedex, France*

Accepted: 1st August 2012

KEYWORDS
Bone microarchitecture;
Texture analysis;
Vertebral fracture;
Calcaneus;
Radius

Summary
Introduction: Osteoporosis is an alteration of bone mass and microarchitecture leading to an increased risk of fractures. A radiograph is a 2D projection of the 3D bone network exposing a texture, that can be assessed by texture analysis. We compared the trabecular microarchitecture of the spine, radius and calcaneus in a series of osteoporotic cadavers.
Materials and methods: Thirty-four cadavers (11 men, 23 women), mean age 85.2 ± 2.1 years, were radiographed from T4 to L5 to identify those with vertebral fractures (FV). Non-fractured vertebrae (NFV), radius and calcaneus were taken and analyzed by densitometry, radiography and texture analysis under run-length, skeletonization of the trabeculae, and fractal geometry.
Results: Six subjects (five women, one man) were selected, mean age 82.5 ± 5.5 years. Twelve calcanei and 10 radii were taken. Two radii were excluded. The texture of NFV was significantly correlated ($P < 0.01$) with that of the radius for horizontal run-lengths. No relationship between the texture of NFV and calcaneus was found.
Discussion: In the horizontal direction (perpendicular to the stress lines), the microarchitecture of NFV and radius showed a disappearance of the transverse rods anchoring the plates. Due to its particular microarchitecture, the calcaneus is not representative of the vertebral status.

* Corresponding author. Tel.: +33 244 68 83 49; fax: +33 244 68 83 50.
E-mail address: daniel.chappard@univ-angers.fr (D. Chappard).

1877-0568/$ - see front matter © 2012 Elsevier Masson SAS. All rights reserved.
doi:10.1016/j.otsr.2012.08.004

Conclusion: Bone densitometry provides no information about microarchitecture. Texture analysis of X-ray images of the radius would be a minimally invasive tool, providing an early detection of microarchitectural alterations.
Level of evidence: IV retrospective study.
© 2012 Elsevier Masson SAS. All rights reserved.

Introduction

Osteoporosis is a global public health problem. Among 100 French women who are now reaching the age of 50, 40 will have a fragility fracture; similarly, one out of eight men will present at least one. Osteoporotic fractures, classified according to their prevalence, are those of the proximal femur (61%), wrist (28%), humerus (11%) [1], and vertebrae. The assessment of vertebral fractures (FV) is difficult: they are often asymptomatic and difficult to diagnose. Osteoporosis has long been considered solely a question of low bone mass based on histomorphometry [2] or densitometry [3]. In 1993 and 2001, WHO added the concept of ''microarchitectural changes'' leading to decreased bone strength and leading to an increased risk of fractures [4,5]. Bone strength reflects both bone mass, appreciable by absorptiometry Bone Mineral Density (BMD) and bone quality. The latter is now understood as a set of factors conferring biomechanical characteristics to bones: macroarchitecture and microarchitecture but also hardness, elasticity, mineralization degree, etc. [6].

Bone, as a ''living biomaterial'', is not randomly distributed but trabeculae are aligned along the stress lines (Wolff's law) [7,8]. There are noticeable differences between trabecular and cortical bone. In trabecular bone, trabeculae can take two shapes, plates connected by transverse rods [9]. Cortical bone appears denser and composed of haversian systems centered on a canal whose direction is parallel to the strains. In osteoporosis, trabecular microarchitecture is altered earlier than bone mineral density [10,11]. However, vertebral microarchitecture is difficult to analyze clinically: computed tomography, which produces 3D analyses, delivers high radiation doses. It would be helpful to evaluate, with an easily accessible technique, an appendicular bone having a microarchitecture close to the vertebra.

Radiography is currently used in medical practice; the resulting images are two-dimensional projections and the trabecular bone network appears as a complex pattern. Digitized X-ray images are usually encoded in 256 gray levels, thus allowing access to data evaluable by mathematical techniques based on texture analysis that the human eye cannot evaluate [12,13].

The aims of this study were to evaluate the trabecular microarchitecture of the vertebra and two appendicular bones (distal radius and calcaneus) by texture analysis in a series of anatomical subjects with at least one osteoporotic FV. The analysis was performed on the adjacent non-fractured vertebrae (NFV). Our hypothesis was that the radius, which has a microarchitecture close to that of the vertebra, could be used to evaluate microarchitecture in osteoporotic patients.

Materials and methods

Population studied

Thirty-four subjects from the anatomy laboratory were studied: 11 men and 23 women. The average age was 85.2 ± 2.1 years. Each subject had given his/her body to science. All were radiographed in profile with an OEC® 7700 Compact camera (GE Medical Systems) to identify those with FV defined as a > 20% decrease in height of the vertebral body (grades 1, 2 and 3 according to the classification of Genant [14]). Seven cadavers with FV were selected: six women, one man (mean age 81.1 ± 4.9 years). One woman was excluded for a FV of metastatic origin at T12.

Removal of bones: vertebrae and appendicular bones

Removal of the vertebrae

The subject was installed in the ventral decubitus. The fractured vertebra was located by fluoroscopy and a pin was placed into the processus spinosus of the vertebra. A median posterior approach, centered on the processus spinosus, was performed. Laminectomy, centered on the FV and the adjacent vertebrae was done. A block of vertebrae including the FV and the adjacent NFV was then removed.

Removal of radius

After having done a Henry's incision, pronator teres and pronator quadratus were separated from bone surface with a rasp and the membrane was cut along the ulnar border of the radius. The radius were sawed on the right and left sides at the junction of the distal and middle thirds.

Removal of the calcaneus

The various tendon and muscle insertions were detached from the calcaneus on the right and left legs. The ankle joint was dislocated, allowing resection of talo-calcaneal block.

Bone cleaning

For each specimen, a gross excision of the adherent soft tissues (ligaments, tendons...) was done [15]. Then they were treated for 48 hours by alternating sodium hypochlorite (diluted to 30% in water) and a high pressure jet of hot water, allowing the removal of the remaining soft tissues.

Bone microarchitecture analysis

X-ray examination of specimens

Each specimen was X-rayed on a high-resolution Faxitron MX-20 (Edimex, Angers, France) to perform a radiogrammetric analysis and a texture analysis (NFV, radius and calcaneus). All specimens were in direct contact with the CCD camera to limit image distortion and compare images at the same magnification. The images were coded into eight bits (256 levels of gray, black = 0, white = 255).

Vertebral radiogrammetry

A spinal radiogrammetry software was developed on a Quantimet 550 image analyzer (Leica, Rueil-Malmaison, France) to assess the stage of deformation by measuring the different vertebral heights: anterior (Ha), middle (Hm), posterior (Hp), antero-posterior (APR), medio-posterior (MPR), and the vertebral surface according to Genant [14]. Only NFV were selected (as corresponding to a grade 0) since they were subjected to the same mechanical conditions that FV (grades 2 and 3, not included here) (Fig. 1).

Texture analysis

For each vertebra, a region of interest (ROI) of 512×512 pixels was selected on the radiograph. The ROI was always positioned in the posterior-central area of the vertebra and was only composed of trabecular meshwork (Fig. 2A). A ROI was positioned in the metaphyseal region of the distal radius, and the ROI was placed at the junction of the body and tuberosity of the calcaneus. The ROIs were always kept away from the subchondral bone and cortices as these two locations in the appendicular skeleton are composed of bones with different trabecular trajectories [16].

Texture analysis methods used here were based on Euclidean and fractal geometry and the mathematical bases have been presented elsewhere [17—19]. A routine algorithm was used to eliminate the X-ray blur prior to analysis; this reduced exposure irregularities and provided sharper and more homogeneous images (Fig. 2B). The following parameters were measured:

- run-length of the gray levels (a run representing a set of pixels all having the same gray level):
  - short run emphasis (SRE). If SRE is high, the texture is fine,
  - long run emphasis (LRE). If LRE is high, the texture is coarse,
  - gray level non-uniformity (GLN). If GLN is high, the number of runs with identical gray levels increases,
  - run-length non-uniformity (RLN). If RLN is high, the gray levels are unevenly distributed between the runs,
  - run percentage (RP). If RP is high, the texture is inhomogeneous and consists of numerous small runs,
  - low gray level runs emphasis (LGRE). If LGRE is high, the image is composed of runs with a low gray level (close to black),
  - high gray level runs emphasis (HGRE). If HGRE is high, the image is composed of runs with a high gray level (close to white).

  These parameters were analyzed in the horizontal (h) and vertical (v) direction for each specimen.

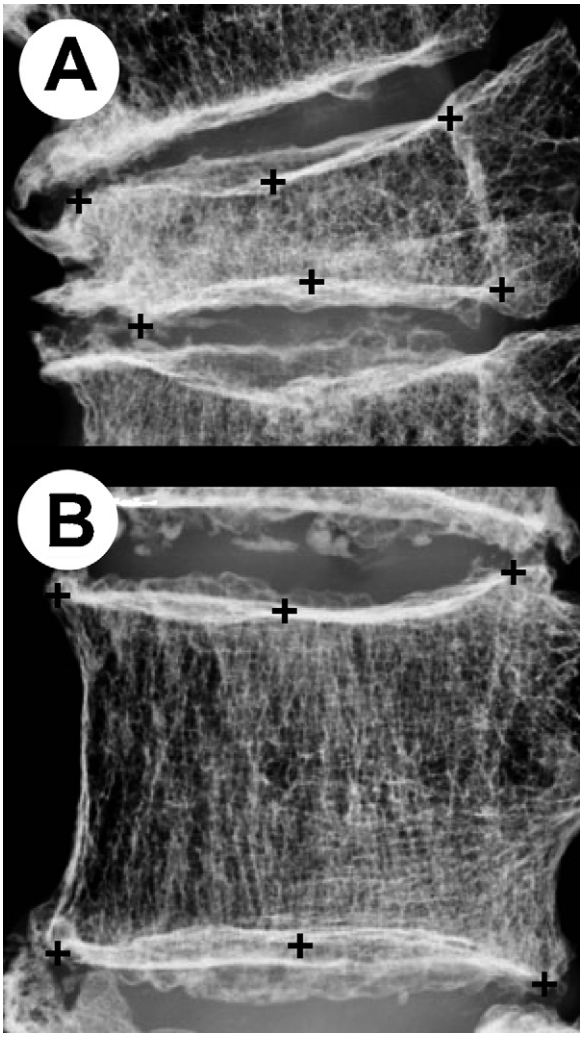

Figure 1 Radiogrammetry of the vertebrae. A. Fractured vertebra (FV) excluded from the study. B. Non-fractured vertebra (NFV) retained. The crosses are placed at the top or bottom corners of the vertebral bodies and in the middle of the endplates.

- skeletonization of the images: trabeculae are thresholded and skeletonized (i.e. reduced to a single line of watershed) by algorithms based on mathematical morphology (Fig. 2C). We measured the following parameters according to Geraets [20]:
  - area: representing the fractional surface area of white pixels,
  - axis: is the surface area of the white skeleton,
  - ends and Nodes are respectively the number of nodes and free ends of the white skeleton,
  - circ: is the total number of white pixels with a black neighbor;
- by using fractal geometry, we measured the fractal dimension with the skyscrapers method (D_{SKY}) (Fig. 2D) and dynamic blankets using two structuring elements gliding in the image: a cross and a vector. The fractal dimension obtained with the cross (D+) and those obtained with a horizontal (D—) or vertical (D$\vert$) vector were determined.

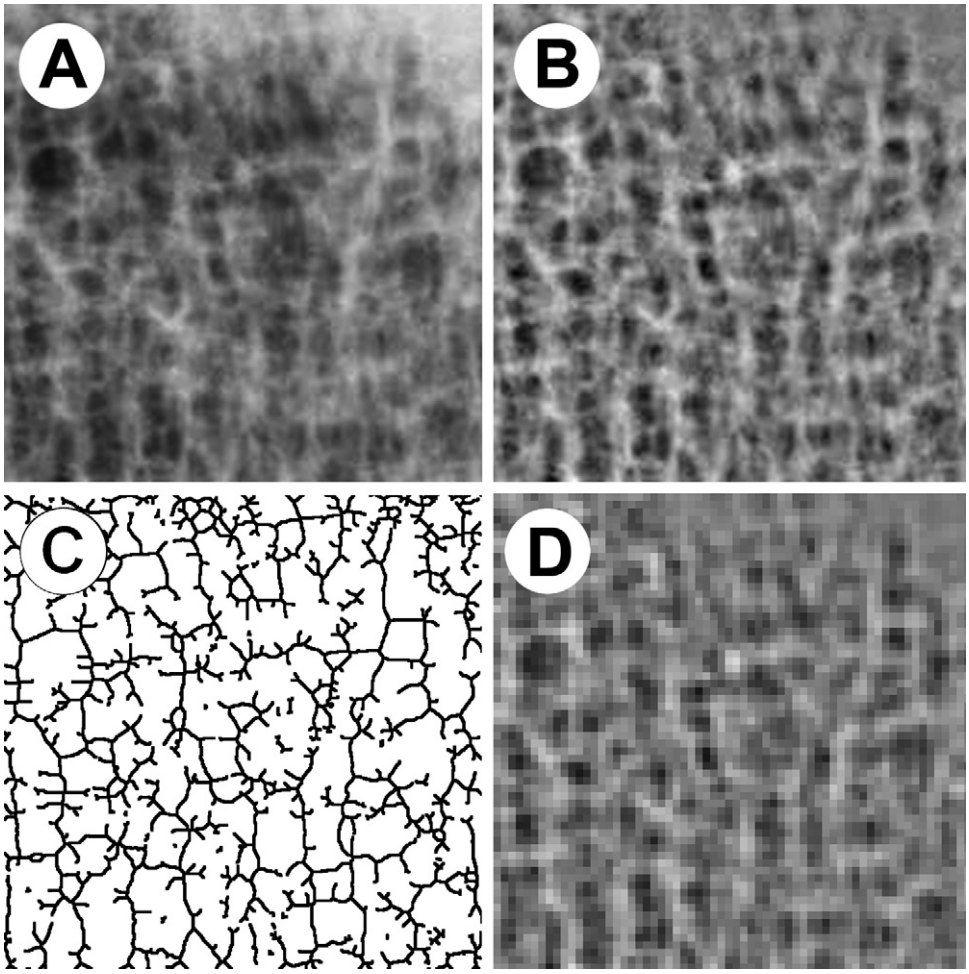

Figure 2 Texture analysis applied to the trabecular bone of a non-fractured vertebrae (NFV). A. Raw radiographic image. B. Image after X-ray deblurring. C. Skeletonization of the trabeculae. D. Fractal analysis by the skyscrapers method.

For each subject, the average values measured on the NFV were chosen. For the appendicular bones, the parameters were measured on the left and right side and the average of the both sides was compared to the vertebrae' values.

Analysis of the bone mineral density

Bone densities of appendicular bones were measured by dual photon absorptiometry (Hologic Discovery AS/N 82425). They were placed in a plastic container containing water whose volume was kept constant during all measurements. A ROI of 60×15 mm was determined at the distal metaphysis of the radius and 70×20 mm at the calcaneus body. The ROI was of the same size than that used for the texture analysis. BMD (in g/cm^2) was measured with the manufacturer's software with the subregion spine analysis module.

Statistical analysis

Statistical analysis was performed using the Systat statistical software release 13.0 (Systat Software Inc., San José, CA). All data were expressed as mean $\pm$ standard error of the mean (SEM). Analysis of variance was performed to test the difference between the different bones followed by post hoc tests for intergroup comparisons. Relationships between parameters were searched by using linear regression analysis (Pearson' r correlation coefficient). Differences were considered significant when $P < 0.05$.

Results

Six subjects were included (mean age 82.5 ± 5.5 years) with osteoporotic FV grades 2 and 3: five women and one man. Twelve calcaneus (six right and six left) were collected. Ten radii were taken (five right, five left). Two radii were excluded: one had a post-fracture callus and another was lost.

Vertebral radiogrammetry

Six subjects presented an established osteoporosis with at least a grade 2 FV. The NFV were grade 0 and were in the close vicinity of FV. Ten NFV were collected.

Bone densitometry of the appendicular bones

BMD was significantly correlated between the right and left side for the calcaneus ($r = 0.92$, $P < 0.009$). The number of

radius was too small to allow a similar statistical analysis. No correlation between bone density of the radius and calcaneus was found.

Texture analysis

Results for the three types of bones are shown in Table 1 (radius *vs*. vertebra), Table 2 (calcaneus *vs*. vertebra) and Table 3 (radius *vs*. calcaneus). At the radius, correlations were found between BMD and some texture parameters (D_{SKY} $r = 0.82$, $P = 0.003$; hRP $r = 0.63$, $P = 0.004$; hRLE $r = 0.65$ $P = 0.04$ and vRLN $r = 0.64$ $P = 0.04$). No relationship was observed at the calcaneus for BMD and texture parameters.

In the NFV, the run-length method showed a significant difference ($P < 0.005$) between the horizontal and vertical analysis for SRE, RP, and LGRE. In the horizontal direction, SRE was significantly higher ($P < 0.0002$), indicating a finer texture than in the vertical direction (parallel to the stress lines). RP was significantly higher in the horizontal direction ($P < 0.0001$), indicating an inhomogeneous texture, made of smaller runs than in the vertical direction. LGRE was significantly lower in the horizontal direction ($P < 0.02$): the image having low values of grey level, away from black. Taken together, the blanket method showed that the trabeculae were more numerous vertically than horizontally. All these data evidenced a loss of transverse horizontal rods used to connect the vertical plate-like trabeculae.

The radius texture was better correlated with that of the vertebra by the run-length method, but only in the horizontal direction for SRE, LRE, GLN, RLN and RP (Fig. 3A). On the other hand, no relationship between vertebrae and calcaneus (Fig. 3B) or between radius and calcaneus was found. Given the low number of subjects and bones, we did not examine whether a left/right correlation existed for these parameters. All these results indicated that the calcaneus microarchitecture did not correlate with that of vertebra and radius. The radius microarchitecture appeared closely related to the vertebra microarchitecture.

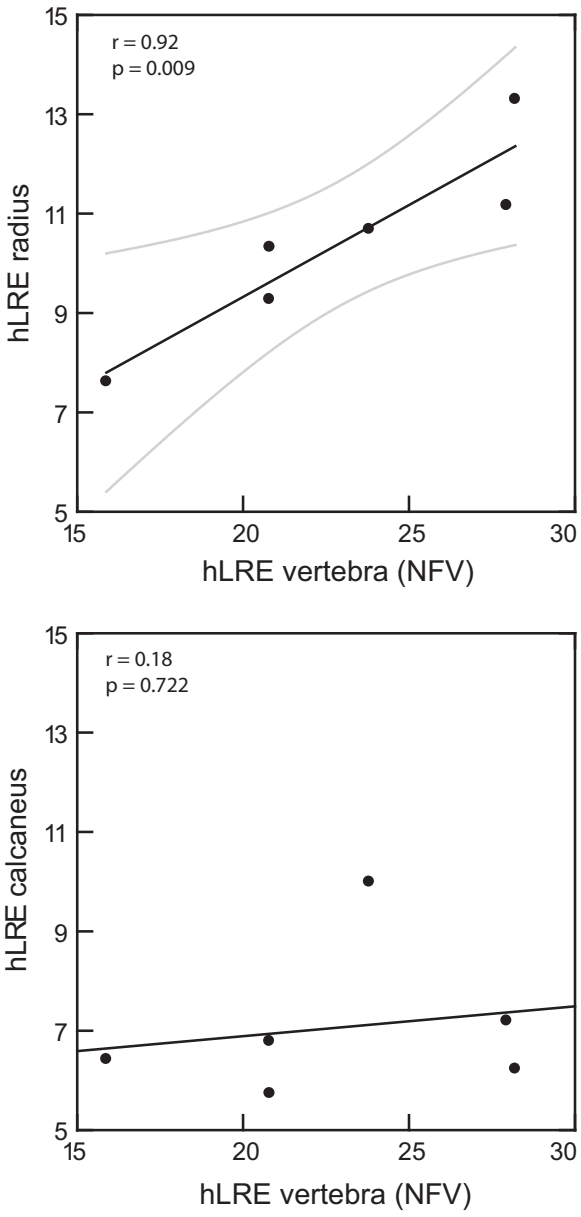

Figure 3 Correlations between parameters hLRE non-fractured vertebrae (NFV) measured in the vertebrae. A. In radius. B. In the calcaneus.

Discussion

In the present study, the texture of trabecular bone in the NFV was significantly correlated with that of radius but not calcaneus. Texture analysis has been used for breast cancer screening [21], in neurology [18], and for the assessment of trabecular microarchitecture in bone diseases [13,22,23]. Bone has the unique ability to adapt its shape and microarchitecture in response to mechanical loads via a process known as remodeling implying the conjoined action of osteoblasts and osteoclasts. Trabecular bone microarchitecture is a key element of the biomechanical strength of bone [24]. Vertebrae and radius have a trabecular microarchitecture composed of horizontal rods which connect large plates that run parallel to the force of gravity. On the other hand, trabecular microarchitecture of the calcaneus realizes intersecting arches which are adapted to the strains exerted in multiple directions.

X-ray images correspond to a 2D projection of the trabecular microarchitecture that is not influenced by the cortices. Texture analysis can help understanding the relationships between pathophysiology of bone loss at different skeletal locations. In osteoporosis, horizontal trabeculae (perpendicular to the stress lines), anchoring the bone plates, disappear in NFV. The same alterations were observed at the radius reflecting the disappearance of horizontal trabeculae. No relationship between vertebrae and calcaneus was shown because trabecular architecture is totally different (resp. horizontal/vertical rods and systems in the form of arches). The low number of radius in this series did not allow a reliable analysis between the right and left sides. Some texture parameters correlate with BMD but, here again, the number of specimens was insufficient.

For some authors, BMD of the calcaneus predicts osteoporotic FVs [25]. However, BMD provides no information on bone microarchitecture, which appears early impaired in osteoporosis. Currently, direct measurement of vertebral

Table 1 Linear correlation between texture parameters measured on radiographs of the radius and non-fractured vertebrae (NFV).

	Radius	NFV	*P*	*r*
Skeletonization analysis				
Ends	0.00324 ± 0.00013	0.0021 ± 0.00013	NS	
Nodes	0.00523 ± 0.00021	0.00359 ± 0.00008	NS	
Run-length analysis				
hSRE	0.487 ± 0.019	0.310 ± 0.028	<0.01	0.934
hLRE	10.398 ± 0.777	22.902 ± 1.936	<0.009	0.921
hGLN	14668.914 ± 292.912	9257.335 ± 275.301	<0.05	0.855
hRLN	27645.856 ± 2451.021	13003.974 ± 1618.662	<0.003	0.958
hRP	0.403 ± 0.015	0.280 ± 0.015	<0.003	0.956
hLGRE	0.0181 ± 0.001	0.025 ± 0.005	NS	
hHGRE	77.552 ± 5.142	69.161 ± 4.071	NS	
vSRE	0.275 ± 0.011	0.232 ± 0.0173	NS	
vLRE	27.179 ± 2.058	33.095 ± 1.730	NS	
vGLN	9235.216 ± 254.540	7626.66 ± 133.660	NS	
vRLN	9821.135 ± 634.939	8567.010 ± 673.523	NS	
vRP	0.253 ± 0.008	0.231 ± 0.008	NS	
vLGRE	0.018 ± 0.001	0.025 ± 0.005	NS	
vHGRE	77.206 ± 5.106	68.816 ± 4.232	NS	
Fractal analysis				
D_{sky}	2.523 ± 0.009	2.456 ± 0.014	NS	
D+	2.411 ± 0.009	2.287 ± 0.007	NS	
D−	2.336 ± 0.005	2.190 ± 0.008	NS	
D|	2.280 ± 0.008	2.199 ± 0.008	NS	

In the last column, the result of the Pearson's coefficient is given when $P < 0.05$. NS: non-significant.

Table 2 Correlation between textural parameters measured on radiographs of the calcaneus and non-fractured vertebrae (NFV).

	Calcaneus	NFV	*P*	*r*
Skeletonization analysis				
Ends	0.00678 ± 0.00028	0.00211 ± 0.00013	NS	
Nodes	0.01176 ± 0.00037	0.00360 ± 0.00008	0.05	0.806
Run-length analysis				
hSRE	0.571 ± 0.015	0.310 ± 0.0278	NS	
hLRE	7.064 ± 0.620	22.902 ± 1.936	NS	
hGLN	19285.205 ± 531.457	9257.335 ± 275.301	NS	
hRLN	40782.741 ± 2824.228	13003.973 ± 1618.662	NS	
hRP	0.478 ± 0.015	0.280 ± 0.015	NS	
hLGRE	0.017 ± 0.001	0.025 ± 0.005	NS	
hHGRE	77.082 ± 3.864	69.161 ± 4.071	NS	
vSRE	0.644 ± 0.005	0.232 ± 0.017	NS	
vLRE	5.053 ± 0.177	33.095 ± 1.730	NS	
vGLN	21970.642 ± 302.401	7626.660 ± 133.662	NS	
vRLN	56806.546 ± 1409.893	8567.010 ± 673.523	NS	
vRP	0.550 ± 0.006	0.231 ± 0.008	NS	
vLGRE	0.017 ± 0.001	0.025 ± 0.005	NS	
vHGRE	77.189 ± 3.807	68.816 ± 4.232	NS	
Fractal analysis				
D_{sky}	2.653 ± 0.010	2.456 ± 0.014	NS	
D+	2.658 ± 0.008	2.287 ± 0.007	NS	
D−	2.450 ± 0.010	2.190 ± 0.008	NS	
D|	2.495 ± 0.008	2.199 ± 0.008	NS	

In the last column, the result of the Pearson's coefficient is given when $P < 0.05$. NS: non-significant.

Table 3 Correlation between textural parameters measured on radiographs of the radius and calcaneus.

	Radius	Calcaneus	*P*	*r*
Skeletonization analysis				
Ends	0.00324 ± 0.00013	0.00678 ± 0.00028	NS	
Nodes	0.00523 ± 0.00021	0.01176 ± 0.00037	NS	
Skeletonization analysis				
hSRE	0.487 ± 0.019	0.571 ± 0.014	NS	
hLRE	10.398 ± 0.777	7.064 ± 0.62	NS	
hGLN	14668.914 ± 292.912	19285.205 ± 531.457	NS	
hRLN	27645.857 ± 2451.021	40782.741 ± 2824.228	NS	
hRP	0.403 ± 0.015	0.478 ± 0.015	NS	
hLGRE	0.018 ± 0.001	0.017 ± 0.001	NS	
hHGRE	77.552 ± 5.142	77.082 ± 3.864	NS	
vSRE	0.275 ± 0.010	0.644 ± 0.005	NS	
vLRE	27.179 ± 2.058	5.053 ± 0.177	NS	
vGLN	9235.216 ± 254.54	21970.642 ± 302.401	NS	
vRLN	9821.135 ± 634.939	56806.546 ± 1409.893	NS	
vRP	0.253 ± 0.008	0.549 ± 0.006	NS	
vLGRE	0.018 ± 0.001	0.017 ± 0.001	NS	
vHGRE	77.206 ± 5.106	77.189 ± 3.807	NS	
Fractal analysis				
D_{sky}	2.523 ± 0.009	2.653 ± 0.009	NS	
D+	2.411 ± 0.009	2.657 ± 0.008	NS	
D−	2.336 ± 0.005	2.451 ± 0.009	0.05	0.814
D|	2.279 ± 0.008	2.495 ± 0.008	NS	

In the last column, the result of the Pearson's coefficient is given when $P < 0.05$. NS: non-significant.

bone microarchitecture is difficult other than by X-ray tomography or MRI. Moreover, in these two methods, the pixel size is larger than that of the trabecuarr thickness. Recently, high resolution peripheral quantitative computed tomography has been proposed at the distal tibia and radius but the method remains to be validated for clinical use [25]. MRI studies have confirmed that microarchitecture analysis at the distal radius is representative of the spine [26]. In addition, a recent meta-analysis of different types of bones confirmed that the magnitudes of strains between the vertebra and radius are closely related (respectively 1350 m and 1420 m) but are different from the values of the calcaneus (5500 m) [27]. In this study, despite the low number of subjects, texture analysis of X-ray images seems a useful noninvasive tool for exploring microarchitecture. The distal radius is an easily accessible peripheral bone whose values are well correlated to those of the vertebrae. This could serve as a test for the assessment of bone microarchitecture in addition to dual-energy absorptiometry.

There are some limitations to the present study. First, the number of subjects is low and no relationship between microarchitectural parameters at the vertebra and the calcaneus was observed. However, it should be pointed out that conflicting results on the relationships between these two bones appear in the literature [28,29]. On the other hand, relationships between microarchitectural parameters at the radius and vertebra have been reported by others with computed tomography [26]. Secondly, the specimens used here were extensively defatted and defleshed. Fat is known to interfere with all types of X-ray examinations including texture analysis but the changes are modest [30].

Conclusion

Bone densitometry, which is the current ''gold standard'' method for the evaluation of osteoporosis, provides no information on the microarchitecture deterioration, which is prematurely damaged. Some authors have reported the use of a score related to microarchitecture and computable on densitometry images but its reliability has been recently questioned [31]. In osteoporosis, the appendicular bone whose architecture is the closest to that of the vertebra is the distal radius, which presents a similar disappearance of the rods anchoring the transverse plates. Texture analysis of X-ray images of the distal radius would represent an easy accessible non-invasive tool to appreciate the early microarchitectural alterations in osteoporosis.

Disclosure of interest

The authors declare that they have no conflicts of interest concerning this article.

Acknowledgements

This work was made possible through the regional contract Bioregos2 Pays de la Loire. F.M. won a master award from SOFCOT in 2011. We thank Professor Maurice Audran, and M. Yannick Simon for their help in this study.

References

[1] Maravic M, Le Bihan C, Landais P, Fardellone P. Incidence and cost of osteoporotic fractures in France during 2001. A methodological approach by the national hospital database. Osteoporos Int 2005;16:1475—80.

[2] Meunier PJ, Courpron P, Edouard C, Bernard J, Bringuier JP. Physiological senile involution and pathological rarefaction of bone. Quantitative and comparative histological data. Br Med J 1973;2:239—56.

[3] Kanis JA, Melton 3rd LJ, Christiansen C, Johnston CC, Khaltaev N. The diagnosis of osteoporosis. J Bone Miner Res 1994;9:1137—41.

[4] Anonymous. Osteoporosis prevention, diagnosis, and therapy. JAMA 2001;285:785—95.

[5] Anonymous. Consensus development conference. Prophylaxis and treatment of osteoporosis. Am J Med 1993;94:646—50.

[6] Felsenberg D, Boonen S. The Bone Quality Framework: determinants of bone strength and their interrelationships, and implications for osteoporosis management. Clin Ther 2005;27:1—11.

[7] Frost HM. Skeletal structural adaptations to mechanical usage (SATMU): 2. Redefining Wolff's law: the remodeling problem. Anat Rec 1990;226:414—22.

[8] Frost HM. Bone ''mass'' and the ''mechanostat'': a proposal. Anat Rec 1987;219:1—9.

[9] Whitehouse WJ. The quantitative morphology of anisotropic trabecular bone. J Microsc 1974;101:153—68.

[10] Libouban H, Moreau MF, Legrand E, Baslé MF, Audran M, Chappard D. Comparison insight dual X-ray absorptiometry (DXA), histomorphometry, ash weight, and morphometric indices for bone evaluation in an animal model (the orchidectomized rat) of male osteoporosis. Calcif Tissue Int 2001;68:31—7.

[11] Brandi ML. Microarchitecture, the key to bone quality. Rheumatology (Oxford) 2009;48(Suppl. 4):iv3—8.

[12] Chappard D, Chennebault A, Moreau M, Legrand E, Audran M, Baslé MF. Texture analysis of X-ray radiographs is a more reliable descriptor of bone loss than mineral content in a rat model of localized disuse induced by the Clostridium botulinum toxin. Bone 2001;28:72—9.

[13] Lespessailles E, Chappard C, Bonnet N, Benhamou CL. Imaging techniques for evaluating bone microarchitecture. Joint Bone Spine 2006;73:254—61.

[14] Genant HK, Wu CY, van Kuijk C, Nevitt MC. Vertebral fracture assessment using a semiquantitative technique. J Bone Miner Res 1993;8:1137—48.

[15] Boyde A. Scanning electron microscope studies on bone. In: Bourne GH, editor. The biochemistry and physiology of bone. NY: Academic Press; 1972. p. 259—310.

[16] Lespessailles E, Poupon S, Niamane R, Loiseau-Peres S, Derommelaere G, Harba R, et al. Fractal analysis of trabecular bone texture on calcaneus radiographs: effects of age, time since menopause and hormone replacement therapy. Osteoporos Int 2002;13:366—72.

[17] Chappard D, Degasne I, Huré G, Legrand E, Audran M, Baslé MF. Image analysis measurements of roughness by texture and fractal analysis correlate with contact profilometry. Biomaterials 2003;24:1399—407.

[18] Szczypinski PM, Strzelecki M, Materka A, Klepaczko A. MaZda-a software package for image texture analysis. Comput Methods Programs Biomed 2009;94:66—76.

[19] Galloway MM. Texture analysis using gray level run lengths. Comput Graph Image Proc 1975;4:172—9.

[20] Geraets WGM, Van Der Stelt PF, Netelenbos CJ, Elders PJM. A new method for automatic recognition of the radiographic trabecular pattern. J Bone Miner Res 1990;5:227—33.

[21] Karahaliou A, Skiadopoulos S, Boniatis I, Sakellaropoulos P, Likaki E, Panayiotakis G, et al. Texture analysis of tissue surrounding microcalcifications on mammograms for breast cancer diagnosis. Br J Radiol 2007;80:648—56.

[22] Messent EA, Ward RJ, Tonkin CJ, Buckland-Wright C. Tibial cancellous bone changes in patients with knee osteoarthritis. A short-term longitudinal study using Fractal Signature Analysis. Osteoarthritis Cartilage 2005;13:463—70.

[23] Cortet B, Chappard D, Boutry N, Dubois P, Cotten A, Marchandise X. Relationship between computed tomographic image analysis and histomorphometry for microarchitectural characterization of human calcaneus. Calcif Tissue Int 2004;75:23—31.

[24] Chappard D, Baslé MF, Legrand E, Audran M. Trabecular bone microarchitecture: a review. Morphologie 2008;92: 162—70.

[25] Kazakia GJ, Hyun B, Burghardt AJ, Krug R, Newitt DC, de Papp AE, et al. In vivo determination of bone structure in postmenopausal women: a comparison of HR-pQCT and high-field MR imaging. J Bone Miner Res 2008;23:463—74.

[26] Link TM, Bauer J, Kollstedt A, Stumpf I, Hudelmaier M, Settles M, et al. Trabecular bone structure of the distal radius, the calcaneus, and the spine: which site predicts fracture status of the spine best? Invest Radiol 2004;39:487—97.

[27] Al Nazer R, Lanovaz J, Kawalilak C, Johnston JD, Kontulainen S. Direct in vivo strain measurements in human bone-a systematic literature review. J Biomech 2012;45:27—40.

[28] Trebacz H, Natali A. Ultrasound velocity and attenuation in cancellous bone samples from lumbar vertebra and calcaneus. Osteoporos Int 1999;9:99—105.

[29] Amling M, Herden S, Posl M, Hahn M, Ritzel H, Delling G. Heterogeneity of the skeleton: comparison of the trabecular microarchitecture of the spine, the iliac crest, the femur, and the calcaneus. J Bone Miner Res 1996;11:36—45.

[30] Chappard D, Pascaretti-Grizon F, Gallois Y, Mercier P, Baslé MF, Audran M. Medullar fat influences texture analysis of trabecular microarchitecture on X-ray radiographs. Eur J Radiol 2006;58:404—10.

[31] Bousson V, Bergot C, Sutter B, Levitz P, Cortet B. Trabecular bone score (TBS): available knowledge, clinical relevance, and future prospects. Osteoporos Int 2011;23: 1489—550.